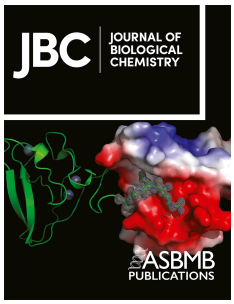

Identification and characterization of 2nd generation EZH2 inhibitors with extended residence times and improved biological activity

Jacob I. Stuckey, Nico R. Cantone, Alexandre Côté, Shilpi Arora, Valerie Vivat, Ashwin Ramakrishnan, Jennifer A. Mertz, Avinash Khanna, Jehrod Brenneman, Victor S. Gehling, Ludivine Moine, Robert J. Sims, III, James E. Audia, Patrick Trojer, Julian R. Levell, Richard T. Cummings

PII: S0021-9258(21)00121-6

DOI: https://doi.org/10.1016/j.jbc.2021.100349

Reference: JBC 100349

To appear in: *Journal of Biological Chemistry*

Received Date: 15 October 2020

Revised Date: 21 January 2021

Accepted Date: 26 January 2021

Please cite this article as: Stuckey JI, Cantone NR, Côté A, Arora S, Vivat V, Ramakrishnan A, Mertz JA, Khanna A, Brenneman J, Gehling VS, Moine L, Sims RJ III, Audia JE, Trojer P, Levell JR, Cummings RT, Identification and characterization of 2nd generation EZH2 inhibitors with extended residence times and improved biological activity, *Journal of Biological Chemistry* (2021), doi: https://doi.org/10.1016/j.jbc.2021.100349.

Identification and characterization of 2nd generation EZH2 inhibitors with extended residence times and improved biological activity

Jacob I. Stuckey,[1,2] Nico R. Cantone,[1] Alexandre Côté,[1,3] Shilpi Arora,[1,4] Valerie Vivat,[1] Ashwin Ramakrishnan,[1,5] Jennifer A. Mertz,[1,2] Avinash Khanna,[1,6] Jehrod Brenneman,[1,7] Victor S. Gehling,[1] Ludivine Moine,[1,8] Robert J. Sims III,[1,2] James E. Audia,[1, 2] Patrick Trojer,[1] Julian R. Levell,[1] Richard T. Cummings[1*]

[1]Constellation Pharmaceuticals, Cambridge, MA 02142 USA

Present Address:

[2]Third Rock Ventures, Boston, MA 02116 USA

[3]Schrodinger, New York, NY 10036 USA

[4]Exo Therapeutics, Cambridge, MA 02139 USA

[5]Bristol-Myers Squibb, Cambridge, MA 02142 USA

[6]Hansoh Bio, Rockville, Maryland 20850 USA

[7]Bridge Biotherapeutics, Inc., Cambridge, MA 02142 USA

[8]Blueprint Medicines, Cambridge, MA 02139 USA

[*]Corresponding author: Richard T. Cummings

E-mail: richard.cummings@constellationpharma.com

Running title: Kinetic characterization of potent EZH2 inhibitors

Keywords- residence time, small molecule kinetics, femtomolar, EZH2, TR-FRET binding kinetics

Abstract

The histone methyltransferase EZH2 has been the target of numerous small molecule inhibitor discovery efforts over the last 10+ years. Emerging clinical data have provided early evidence for single agent activity with acceptable safety profiles for 1st Generation inhibitors. We have developed kinetic methodologies for studying EZH2-inhibitor binding kinetics that have allowed us to identify a unique structural modification that results in significant increases in the drug-target residence times of all EZH2 inhibitor scaffolds we have studied. The unexpected residence time enhancement bestowed by this modification has enabled us to create a series of 2nd Generation EZH2 inhibitors with sub-pM binding affinities. We provide both biophysical evidence validating this sub-pM potency as well as biological evidence demonstrating the utility and relevance of such high affinity interactions with EZH2.

Introduction

A diverse array of histone post-translational modifications contribute to the dynamic regulation of chromatin architecture. Discrete combinations of these modifications have been proposed to form a putative "histone code" that can be read out by effector proteins and complexes, to regulate transcription by controlling access to individual genomic loci (1-3). Aberrant alterations in histone coding mechanisms have been extensively linked to the altered transcriptomes observed in tumors (4). Further, genetic alterations in chromatin regulatory proteins are among the most frequent mutational events observed across numerous cancer types (5). Accordingly, there is significant therapeutic interest in pharmacological modulation of key chromatin regulatory proteins (6,7).

The multi-subunit Polycomb Repressive Complex 2 (PRC2) is a key chromatin regulator that exhibits histone methyltransferase activity on H3 lysine 27 (H3K27). The catalytic core of PRC2 consists of a SAM-dependent histone methyltransferase (either EZH1 or EZH2), an H3K27me3-binding subunit (EED) and a Zn-finger, scaffolding subunit (SUZ12). Multiple heterozygous point mutations have been observed in the EZH2 subunit of PRC2. These mutations are a recurrent genomic feature observed in multiple cancer types, with the highest frequency presenting in Non-Hodgkin's Lymphoma (8). Biochemically, these mutations alter the catalytic activity of EZH2, thereby resulting in aberrant, EZH2-mediated global increases in H3K27me3 levels (9-11). Furthermore, EZH2 catalytic function has been implicated more broadly in oncology with EZH2-mediated gene silencing contributing not only to oncogenic pathway activation but also to acquired drug resistance and suppression of anti-tumor immune responses in T-cells (8,12). Accordingly, EZH2 catalytic inhibition is being explored clinically as a therapeutic approach in multiple solid tumor and hematological malignancies with Tazemetostat recently being the first approved EZH2 targeting drug for use in epithelioid sarcoma (7,13-15).

Clinical agents that target EZH2 exert their effect through one of two mechanisms of inhibition. The first inhibitors described belong to multiple series of pyridone-containing small molecules (EZH2i) that target a pocket located near the interface of EZH2 and EED. The critical nature of the pyridone moiety was made clear after multiple reports emerged detailing co-crystal structures of several of these inhibitors with PRC2. These analyses revealed that the sole point of overlap between the compound-binding pocket on EZH2 and the SAM binding site was the area occupied by the pyridone of the respective compounds. This structural insight not only illuminated the previously unknown physical basis for the compounds' SAM-competitive mechanism of inhibition but also cemented the central role of the pyridone in the context of these EZH2 inhibitors (16-18). Some of the more recent PRC2 inhibitor reports have focused on the biochemical role of H3K27me3 binding to the EED subunit of PRC2. The H3K27me3-EED binding event in the context of PRC2 is well-characterized as an allosteric stimulator of EZH2 methyltransferase activity

(19,20). Accordingly, small molecules that potently antagonize the EED-H3K27me3 interaction also allosterically inhibit EZH2 catalytic function. The clinical utility of EED-targeted small molecules is yet to be determined, but pre-clinically, these molecules have resulted in tumor growth inhibition similar to that observed for SAM-competitive PRC2 inhibitors (15,21,22). Meanwhile, multiple SAM-competitive EZH2 inhibitors have demonstrated clinical activity in the absence of dose-limiting toxicities (13). Observation of emerging clinical profiles, in addition to pre-clinical studies in murine models has led us to hypothesize that unlocking the full therapeutic potential of EZH2 inhibitors will require molecules that achieve more comprehensive, durable target engagement than can be achieved with existing clinical EZH2 inhibitors.

Recent mechanistic studies into one sub-series of SAM-competitive EZH2 inhibitors has demonstrated that these molecules exhibit slow, tight-binding behavior. Detailed kinetics studies led to estimated binding affinities of <100 pM for allosterically activated PRC2 for the most potent compound characterized (23). Characterization of such high affinity interactions to elucidate Structure-Activity Relationships (SAR) are challenging using traditional, equilibrium-based assay formats. Theoretical treatment of binding equilibria by Matulsky and Mahan in 1983 first noted that the required equilibration time for an interaction with ligand concentrations equal to its K_d, under pseudo-first order conditions, is a function of the drug-target residence time (τ) (24-27). This can result in interactions that will require multiple days of equilibration to accurately assess affinity if the protein-inhibitor complex exhibits sufficiently slow k_{off} values. This concept was recently highlighted in a report detailing biosensor-based kinetic methodologies to quantify single-digit pM affinities in order to circumvent the practical limitations of equilibrium-based biochemical assays (28). Unfortunately, biosensor-based methodologies, such as surface plasmon resonance (SPR), have limited utility in studying PRC2-inhibitor kinetics because of the large complex size, long residence time of EZH2 inhibitors, and the practical limitations of assessing kinetics in the activated state because of non-specific interactions between cationic histone peptides and the gold biosensor surface.

We recently reported residence time enhancement for EZH2 inhibitors as assessed by a jump dilution method utilizing TR-FRET technology (29). Herein, we describe the full scope of biochemical approaches we used to kinetically characterize high-affinity, pyridone-containing EZH2 inhibitors (EZH2i). Key technical nuances not detailed previously are described here that enabled kinetic characterization of second generation EZH2i. Further, in this work, we also expand the methodology for k_{on} determination to enable fully quantitative potency assessments. Finally, we expand on the Structure-Kinetic Relationships (SKR) described previously (29) by showing the universality of the key structural motif to significantly enhance EZH2-inhibitor residence time across all scaffolds tested. The insights from our kinetic studies have enabled us to drive our 2nd generation series SAM-competitive EZH2 inhibitors to sub-pM biochemical potencies that correlate with enhanced tumor cell-killing *in vitro* and *in vivo*.

Results

Enzymatic Jump Dilution Assays

The standard biochemical assay for assessing enzyme-inhibitor residence times is a jump dilution-based methodology in which enzyme and inhibitor are pre-equilibrated at an inhibitor concentration equal to its IC_{90} value as determined in an equilibrium-based biochemical assay (30). The pre-equilibration is followed by a rapid, 100-fold dilution that results in an inhibitor concentration equal to its IC_{10} value. However, the observed sub-nM EZH2i potencies coupled with the relatively slow turnover of H3 by EZH2 (k_{cat} ~25/hr^{-1}) makes dilution to IC_{10} simply impractical. Further, this cannot be compensated for by increasing the concentration of cofactor competitor due to the radioactive assay readout, because radioactive SAM is stored in a sulfuric acid solution which precludes its use at concentrations >~5x K_m without substantially altering buffer pH.

To overcome these challenges, we applied a modified jump dilution methodology in which inhibitors were diluted to their Cheng-Prusoff (31) adjusted IC_{50}^{app} at the highest possible SAM concentration. A mathematical correction was then applied to k_{obs} to account for rebinding during the establishment of equilibria, thus allowing a more accurate residence time estimate (Supplementary Note I). To corroborate our estimated residence time values, we compared them to SPR-determined values using a specialized methodology for analysis of long residence time compounds with a test set of EZH2i including clinical stage compounds and compounds 1-3, **(**Figure 1). Overall, we observed good agreement with the estimated compound residence time for basal PRC2 (complex in the absence of H3K27me3 activator peptide) between the two methodologies in spite of the differing pH (8.5 vs. 7.4) and salt concentrations (0 vs. 150 mM NaCl) of the biochemical and SPR buffers respectively. The most significant outlier in this set can be accounted for because the residence time of GSK126 under these conditions is simply too short to reliably quantitate enzymatically in our assay set up. Ultimately, this modified jump-dilution methodology quickly became inadequate for our purposes as a result of continued increases in EZH2i residence times. This could not be circumvented by simply running longer reactions times due to the limited stability of SAM in aqueous buffers and was further limited by our inability to accurately estimate compound IC_{50} values.

Development of TR-FRET binding assay to measure inhibitor kinetics

In order to circumvent the limitations of using EZH2 catalytic readouts to estimate inhibitor residence times, we developed a time-resolved fluorescence energy transfer (TR-FRET) to directly measure free EZH2 as a function of time using a biotinylated EZH2 inhibitor that was designed based upon literature precedent (biotin-EZH2i, 4, Figure 2A) (32). The interaction between biotin-EZH2i and His-tagged PRC2 is detected using streptavidin allophycocyanin (SA-APC) and an Eu-αHis antibody (Figure 2B). While the final, measured TR-FRET complex is identical to other standard TR-FRET-based binding assays, assay execution with this system is particularly nuanced. This nuance stems from the altered affinity and kinetics of the biotin probe when complexed with SA-APC. In order to avoid the altered equilibration time observed with the SA-APC:Biotin-EZH2i complex and PRC2, we explored the impact of order of addition on detection of free PRC2. In doing so, we identified conditions that result in effectively instantaneous equilibration between biotin-EZH2i with pre-equilibrated Eu-αHis:PRC2 complex. The SA-APC is then added at a concentration for which its saturation of the biotin-probe bound to EZH2 is also effectively instantaneous (Supplementary Figure 1A and 1B). Under these conditions, we were able to quantitatively measure free PRC2 across a concentration range of 1.4-1000 pM with excellent linearity with respect to free PRC2 vs TR-FRET ratio. The signal, and accordingly, its linearity with respect to [PRC2], peaked between 5-10 minutes following SA-APC addition. Both signal and linearity were stable until ~20 minutes post SA-APC addition. Peak linearity was achieved at 11 minutes following SA-APC addition (R^2 >0.99), thus providing an adequate window of time for reagent addition followed by signal readout (Supplementary Figure 2A and 2B).

We utilized this platform for detection of free EZH2 in two different schematics (Supplementary Schemes I and II, respectively): 1) A jump dilution-based format to monitor dissociation of a pre-bound inhibitor over time to determine k_{off} values and 2) A format to monitor compound association with EZH2 over time to determine k_{on} values. For schematic 1, [PRC2] bound to inhibitor or inhibitor-bound fraction can be plotted vs time and fit to a single-phase exponential decay to determine k_{off} (Figure 2C). Importantly, this can be run under dialysis conditions to ensure compound rebinding does not result in an overestimation of the drug-target residence time. Rebinding was found to be significant for EZH2i where τ > 100 hr and for those compounds only data under dialysis conditions is reported. Data treatment for schematic 2 requires additional nuance for accurate characterization (*vide infra*).

EZH2i binding mechanism determination

An example compound titration using schematic 2 is shown in Figure 2D. We tested multiple compounds across multiple scaffolds with a range of k_{off} values (determined using jump dilution procedure outlined in schematic 1). For each of the compounds tested we observed a clear linear relationship in a plot of k_{obs} vs. [I] (Supplementary Figure 3). This relationship is indicative of a single-step binding mechanism (25,26), in contrast not only to the previously proposed two-step binding mechanism of slow-tight binding EZH2i, but also to many other characterized long residence time compounds for other protein targets (23,25). Further, the observed linear relationship of k_{obs} vs [I] was not affected by allosteric activation of PRC2 using H3K27me3 activator peptide (Supplementary Figure 3C and 3D). Finally, we corroborated this observation using both enzymatic methodologies and from the SPR data generated (Supplementary Figure 4).

The final consideration for data treatment in these experiments stems from the fact that the concentrations of inhibitor used for our association experiments approach that of the total concentration of PRC2 in the sample, requiring treatments based on 2nd order reaction conditions. Thus, to obtain estimates of the k_{on} values for the compounds tested, binding curves were fit to the integrated rate equation for a reversible, bimolecular association reaction. The solution to this has been presented numerous times in various forms, with the form used here shown in Supplementary Note II (33-36).

We next compared the agreement of the kinetic parameters using our TR-FRET based methodologies to the values obtained for the test set of compounds evaluated previously by SPR. All kinetic parameters were in excellent agreement between the two methodologies (Figure 2D and 2E), consequently producing similar estimates for compound binding affinities (K_i, Figure 2F). Taken together, these results indicate that our TR-FRET based methodology is suitable for accurately determining compound-PRC2 kinetic parameters and, therefore, binding affinity.

Allosteric modulation of compound potency

Intriguingly, the aforementioned allosteric stimulation of EZH2 from H3K27me3 activator peptide has also been shown to modulate the residence time of EZH2 inhibitors (23), a phenomenon we also observed with compound 5 during the course of our mechanistic studies (Supplementary Figure 3C and 3D). Utilizing our TR-FRET binding assay, we sought to explore this phenomenon across a panel of EZH2 inhibitors. We found that the residence time of every inhibitor increased, although the extent of increase was highly variable (Figure 3A). To date, we have not observed a clear structure-kinetic relationship that can explain the selectivity for activated relative to basal PRC2, but we suspect it is related to the fact that pyridone-based EZH2i also interact with the EED subunit as a result of their binding at an interface between EZH2-EED (16-18).

Intrigued by the observed allosteric modulation of EZH2i residence time, we probed for residence time modulation of CPI-1205 by an EED small molecule antagonist, MAK683. In contrast to experiments with activator peptide (Figure 3A), we did not observe an increase in the residence time of CPI-1205 by MAK683 (Figure 3B). Nonetheless, the presence of an EEDi negated residence time enhancement by addition of activator peptide (Figure 3C). Interestingly, these data directly indicate that EED-targeted small molecules and pyridone-containing EZH2 inhibitors can co-occupy the same PRC2 complex, providing the molecular basis for a simultaneous, orthogonal, PRC2-targeting approach. Notably, as expected from our MOI studies, there was no effect of allosteric stimulation of EZH2 on compound association kinetics (Figure 3D).

In order to potentially gain insight into the biologically relevant PRC2 state, we compared cellular potencies of a panel of EZH2i with their residence time values obtained in the basal or activated state of PRC2. While we found a general correlation with both values, it was stronger with the H3K27me3 mark reduction EC_{50} values in HeLa cells for the compound residence times in the activated state, particularly for the most potent compounds in the panel, suggesting activated PRC2 is the more biologically relevant state (Figure 3E and 3F). Therefore, our subsequent

kinetic studies described here were conducted in the context of activated PRC2.

Residence time enhancement imparted by 4-thiomethyl pyridone

We recently reported that, quite unexpectedly, the residence time of compound 2, the 4-thiomethyl analog of CPI-1205, (Figure 4A), displayed an order of magnitude increase in inhibitor residence time (29) (Figure 4B). Applying our methodology described here for k_{on} determination, we observed that the residence time enhancement observed for compound 2 was not accompanied by any sort of compensation in k_{on} relative to CPI-1205 (Figure 3D); therefore, the extended residence time resulted in an improvement in the overall binding affinity (Figure 4B). This striking observation, coupled with the critical nature of the pyridone moiety for conferring SAM-competitive inhibition of EZH2, drove us to further explore this observation. We performed a focused SKR study in which the substituent at the 4-position of the pyridone was systematically varied between -Me, -Cl, -OMe and -SMe in the context of an alternative, indole-based scaffold related to CPI-1205/compound 2 (Figure 4C). Strikingly, only the -SMe substituent was able to dramatically extend inhibitor residence times on EZH2 (Figure 4D).

Having observed this -SMe effect on two distinct indole-containing scaffolds, we next sought to interrogate the universality of the residence time enhancement by generating 4-thiomethyl analogs of 4 clinical stage EZH2i, in addition to CPI-1205 (Supplementary Figure 5). We found that residence time was dramatically enhanced in the context of each scaffold. The most strongly impacted scaffolds were EPZ-6438 (Tazemetostat) and GSK126 with both scaffolds exhibiting a ~30-fold residence time enhancement when employing a 4-thiomethyl substitution (Figure 4E).

Mechanistic and biophysical validation of EZH2i with femtomolar binding affinity

We plotted the individual kinetic parameters of the compounds profiled (Figures 1-4) vs. the respective pK_i (M) values calculated from those parameters. The kinetically determined K_i values spanned several orders of magnitude and were driven almost exclusively through residence time increases (Figure 5A and 5B). Strikingly, the most potent K_i estimated in this set was sub-pM (13; $\frac{k_{off}}{k_{on}}$ = 130 fM (pK_i (M) = 12.88)), Figure 5A-C). Closer examination of the 4-thiomethyl-containing compound 13 indicates that the compound possesses a residence time on activated PRC2 on the order of several months (Figure 5B-D; τ = 2,300 hrs = ~3.0 months). We confirmed the stability of recombinant pentameric PRC2 in the TR-FRET assay conditions by assessing its catalytic activity over time when stored at 25°C in assay buffer. We found that the complex was very stable in the assay conditions with no loss in catalytic activity observed after 10 days, indicating a half-life for complex stability of months (Supplementary Figure 6).

We also confirmed that the MOI for compound 13 was maintained (SAM-competitive) relative to previous pyridone-containing EZH2i by examining the effect of SAM on its EZH2 association kinetics. Addition of SAM to these experiments resulted in a dose-dependent reduction in k_{on}^{app}. Importantly, we observed excellent agreement with the K_m of SAM (400 nM) for PRC2 and the EC_{50} for SAM-mediated reductions in k_{on}^{app} for 13 (740 nM; Supplementary Figure 7). We also performed mass spectral analysis of compound 13 following an ~2 day incubation with supra-stoichiometric amounts of PRC2, and found that the compound was recovered unmodified, indicating that the extreme residence time of the compound is not achieved through enzymatic processing of the compound (Supplementary Figure 8).

We next sought biophysical corroboration of the extreme potency observed through characterization of compound binding kinetics. We chose to utilize ligand-induced protein thermal stabilization methodologies because of its demonstrated utility in estimating the potency of the biotin-streptavidin interaction (K_d ~1 fM) (37). We selected four compounds, including 13, estimated to have K_i values spanning nearly 3 orders of magnitude. We tested the thermal stabilization of pentameric PRC2 by these

compounds using Differential Scanning Fluorimetry. Under the conditions tested, thermally induced unfolding of PRC2 exhibits multiphasic behavior as evidenced by the 1st derivative of the fluorescence melting curve (Figure 5E). Interestingly, incubation of PRC2 with each of the compounds in our test set resulted in not only a dramatic stabilization of the first melting peak (ΔT_mD = 11.54-15.78°C), but also condensed the melting curve to a single transition (Figure 5E, lower panel). Further, we found that 13 exhibited significantly greater stabilization of PRC2 relative to the other compounds. This observation holds in terms of both overall melting curve stabilization (ΔT_mB of 9.2°C; Figure 5E, upper panel) and the first melting peak in the derivative of the DMSO control melting curves (ΔT_mD = 15.78°C; Figure 5E, lower panel). These data biophysically demonstrate that 13 does, in fact, have a significantly higher affinity interaction with PRC2 than the other compounds tested. Notably, the ΔT_mD value for these compounds did not correlate with pIC_{50} values obtained from a 24-hour enzymatic assay using very dilute PRC2 (15 pM), highlighting the impractical equilibration time required for accurate assessments of such high affinity interactions (Supplementary Figure 9). Crucially however, we found that the ΔT_mD values of these was correlated with pK_i values obtained from our kinetic experiments, providing strong biophysical evidence of our kinetically determined affinity estimates (Figure 5F). Additionally, we found a similar change in T_m and potency rank when assayed in the biochemical assay buffer (Supplementary Figure 10) again suggesting the affinities determined in different buffers were maintained.

Intrigued by the apparent noncovalent nature of inhibition, we sought to further improve the affinity of 13 by constraining the amide linker between the dioxolane heterocycle and the 4-thiomethyl pharmacophore in order to generate CPI-1328 (Figure 6A). This rigidification resulted in an improved potency of CPI-1328 relative to 13 (Figure 6A and 6B). We observed that the potency increases are driven primarily through increases in the residence time of the molecule and not through any significant changes in the measured association rate constant (Figure 6B). The even longer residence time of CPI-1328 prompted us to check residual catalytic activity at the final assessed timepoints in the jump dilution experiment. Importantly, we found that % catalytic activity was in good agreement with the measured amount of liberated PRC2 (Supplementary Figure 11), indicating that PRC2 is recovered unmodified following compound dissociation.

These results strongly argue for a wholly noncovalent interaction between these inhibitors and PRC2. If reversible covalent bond formation was responsible for the femtomolar affinity bestowed by the 4-thiomethyl pyridone, conformational constraint of the 4-thiomethyl pyridone would have been expected to drive affinity increases by properly positioning the functional group for covalent bond formation. Kinetically, this would manifest improved potency *via* the association phase of the interaction, which was not observed (Figure 6). Importantly, the ring cyclization constraint we introduced would not be expected to impact the electronics of the pyridone, which could affect the apparent affinity through impacting both the reactivity of the functionality as well as the stability of a covalently bound species. Therefore, we conclude that the femtomolar binding affinities we have observed for these compounds are achieved through strictly noncovalent interactions.

Cellular and *in vivo* impact of enhanced compound potencies

The extreme affinity observed in our *in vitro* biochemical experiments led us to inquire whether there are any biological implications of these measurements. We first compared compound residence times to the cellular potencies of our compounds in an H3K27me3 mark reduction assay in HeLa cells. While we found a general correlation with cellular EC_{50} values, the relationship between residence time and EC_{50} in this assay appears to asymptotically approach a limit for the EC_{50} value at ~0.5-1 nM (Figure 7A), suggesting this to be the lower limit of this cellular assay and may reflect the total concentration of PRC2 found in HeLa cells, with the most potent compounds effectively titrating the available enzyme. Regardless, this plateau suggests that there is a limit on the extent that residence time

and compound affinity can drive cellular potency in this assay. Importantly however, we also examined the impact of residence time on cell killing in KARPAS-422 cells, a mutant-EZH2 lymphoma model (Figure 7B). In this context, there is a continuously linear correlation between residence time and GI_{50} values that is both striking and strongly suggestive that the extremely long residence times observed in the TR-FRET assay do in fact translate into enhanced tumor cell killing in EZH2-dependent models. In addition, we find that the correlation further tightens when comparing GI_{50} values to the overall binding affinity (Figure 7C).

We therefore sought to explore the impact of sub-pM binding affinities *in vivo* in the context of a KARPAS-422 xenograft model. To do this, we compared the efficacy of the 1st Generation EZH2i, Tazemetostat (K_i = 64 pM), with that of CPI-1328 (K_i = 63 fM). We used doses of 25 mg/kg QD and 160 mg/kg BID for Tazemetostat while using doses of 10 mg/kg and 25 mg/kg QD for CPI-1328, all given PO. The duration of treatment for CPI-1328 and Tazemetostat was 27 and 29 days, respectively. Tumor and plasma PK analysis was performed 1 hr post-dose on Day 12 in all samples (Supplementary Figure 12A and 12B). Direct comparison of the 25 mg/kg QD arms revealed that the total concentration of Tazemetostat observed in the tumors was 730 ng/g (99.1 % PPB). For CPI-1328, the total concentration of compound present in the tumors was ~2-fold less at 350 ng/g (96.6% PPB). Total plasma levels for Tazemetostat at this time point were 6,100 ng/mL. By contrast, total CPI-1328 plasma levels were significantly lower (490 ng/mL). Additionally, we obtained a more detailed plasma PK profile of CPI-1328 in both arms and observed 12 ng/mL remaining 10 hours post dose (25 mg/kg QD) and undetectable levels at 24 hours, indicating a lack of accumulation *in vivo* for either arm of CPI-1328 (Supplementary Figure 12C). In spite of the significantly higher reduction in the H3K27me3 mark and tumor size by CPI-1328, no signs of overt toxicity or changes in bodyweight were observed (Supplementary Figure 12D and E), suggesting that robust target engagement/inhibition of EZH2 is well tolerated.

We applied an MSD ELISA-based PD readout using the tumor samples collected on Day 12 to assess target engagement at each dose *via* reduction in global H3K27me3 levels. Mice treated with CPI-1328 exhibited dose-dependent reduction in H3K27me3 levels with 10 mg/kg QD CPI-1328 causing a 43% reduction in H3K27me3 levels and 25 mg/kg QD CPI-1328 causing an 89% reduction in H3K27me3 levels (Figure 7D). This dose-dependent reduction in intratumoral H3K27me3 levels was accompanied by a dose-dependent tumor regression profile (Figure 7E). Tumor regression in mice treated with 10 mg/kg QD CPI-1328 is observed at approximately Day 12 while mice treated with 25 mg/kg QD CPI-1328 experience much more rapid onset of tumor regression with decreases in tumor volume beginning at approximately Day 5. In stark contrast, no statistically significant reduction in H3K27me3 levels was observed in mice treated with Tazemetostat at 25 mg/kg QD (Figure 7D). Nevertheless, this dose of Tazemetostat did result in a 49% reduction in tumor volume relative to vehicle (Figure 7F). A similar tumor regression profile to that seen with CPI-1328 was observed with Tazemetostat with significantly higher doses given twice as frequently (160 mg/kg BID, Figure 7F). This higher dose was also associated with significant loss of H3K27me3 levels, comparable to that seen in the CPI-1328, 10 mg/kg QD arm. Taken together, these data strongly support our hypothesis that more comprehensive target coverage by an EZH2i is necessary to fully realize the therapeutic benefit of targeting EZH2.

Discussion

A survey of small molecule drugs in 2006 indicated that the median binding constant was approximately 20 nM (38). A drug or drug-like molecule with equilibrium dissociation constant for its intended target at or below 1 nM is typically regarded as a highly potent molecule (39). Therefore, it is reasonable to question the utility of superseding this potency mark. Frequently in drug discovery research, precise characterization of affinities near or below 1 nM can be challenging

and is often foregone in favor of using cell-based assay formats to inform medicinal chemistry campaigns. Our data strongly argue that continued characterization of high affinity interactions can provide novel, unique insight into Structure-Activity Relationships that may be otherwise overlooked in medicinal chemistry campaigns. Namely, although EZH2 has been the subject of a significant number of drug discovery campaigns across multiple pharmaceutical and academic organizations (7,13-15,17,18,21,32,40,41), insight into the uniqueness of the 4-thiomethyl pyridone was only attained through in-depth, mechanistic studies into the kinetics of EZH2i; studies that required development and utilization of the methodologies presented here.

The affinities reported here for our most potent EZH2i rank among the highest reported for synthetic small molecules with estimates for equilibrium dissociation constants of ~10^{-13} M (100 fM) (42). Previous analyses have indicated that the usual "limit" for noncovalent interactions appears to be ~10^{-11} M (10 pM) (39,42). It has been proposed that attaining potencies beyond this empirical barrier requires use of either covalent/semi-covalent intermediates or transition-state analogs (39). We have been able to locate 3 reports of synthetic small molecules with reported sub-pM binding affinities for their intended target, all of which similarly applied kinetic methodologies to obtain their affinity estimates (43-45).

Finasteride is a mechanism-based inhibitor of 5α-Reductase that is converted by the enzyme to an NADP-dihydrofinasteride adduct. This bisubstrate analog was kinetically characterized to exhibit a K_i similar (10^{-13} M) to that seen for the most potent 2nd Generation EZH2i described here. In the context of Finasteride, a chemical transformation occurs that results in the generation of the high affinity intermediate which eventually is released as a reduced form of the parent compound (43). As noted, we do not observe any evidence of a chemical transformation in the context of our 2nd Generation EZH2i. Instead, our studies are consistent with a fully reversible, presumably noncovalent interaction with a K_i of ~10^{-13} M.

We are aware of only two noncovalent inhibitor studies demonstrating such a high affinity interaction. The first involves high affinity analogs of intermediates in the Spinach Ribulose 1,5-Bisphosphate Carboxylase reaction coordinate (K_i ~190 fM) (44). The second is a transition-state analog, tripeptide phosphonate inhibitor of the zinc-dependent carboxypeptidase A. Affinity estimates for this molecule were ~10-20 fM. At the time, this was speculated to be the most potent inhibition constant for a low molecular weight inhibitor and to our knowledge, remains such (45). Further, a co-crystal structure for this inhibitor has been solved and clearly demonstrates a noncovalent interaction anchored by the phosphonate-Zn interaction, establishing the attainability of noncovalent, femtomolar small molecule inhibitors (46).

Significantly, our most potent 2nd generation EZH2i are distinct from each of these cases in that they do not show evidence of enzymatic processing nor are they analogs of a reaction intermediate. Further, they are unlikely to be transition-state analogs. The available crystallographic evidence for other pyridone-containing inhibitors indicates that these inhibitors do not bind near enough to the actual active site to function as a transition-state mimetic (16-18). In the absence of direct structural information, one of our current hypotheses for the potency enhancements bestowed by the -SMe functionality is the result of the introduction of Sulfur-π interactions with Phe665 and Phe686 based on the aforementioned co-crystal structures of other pyridone-based inhibitors with EZH2. This interaction has been garnering increasing interest for its role in noncovalent interactions but may certainly only be one contributing factor (47,48).

In summary, our 2nd Generation EZH2i are among the most potent described to date for a synthetic small molecule. Further, they represent, to our knowledge, the most potent inhibitors described which do not rely on enzymatic processing or reaction intermediate/transition-state mimicry. Our xenograft studies clearly demonstrate that accessing such high affinity molecules improves their ability to more comprehensively engage EZH2, thereby significantly reducing the drug burden in hyper-sensitive contexts. The continued depression of H3K27me3 levels by 25 mg/kg QD of CPI-1328 vs the same compound given 10

mg/kg QD indicates that even in this hyper-sensitive context, near complete target engagement is required to access the therapeutic potential of EZH2i. We intend to further report on medicinal chemistry optimizations of thiomethyl-containing EZH2i to improve their *in vivo* utility as well as utilization of the femtomolar potencies of our inhibitors to potentially expand the clinical utility of EZH2 inhibitors.

Experimental procedures

Enzymatic assay

Inhibitor potency was assessed through incorporation of 3H-SAM into a biotinylated H3 peptide. Pentameric PRC2 composed of EZH2, EED, SUZ12, RbAp46 and RbAp48 was prepared in-house as described previously (49). (Except for SPR experiments described below all experiments utilized pentameric PRC2.) All peptides were custom synthesized (New England Peptide). Specifically, PRC2 (40 pM), 3H-SAM (0.9 µM; Perkin Elmer), and 2 µM H3K27me3 activating peptide (H_2N-RKQLATKAAR(Kme3)SAPATGGVKKP-amide), in a buffer consisting of 50 mM Tris (pH 8.5), 1 mM DTT, 0.07 mM Brij-35, and 0.1 mg/mL BSA, was added at 12.5 µL/well to 384 well plates (Greiner) containing 0.2 µL droplets of acoustically-dispensed inhibitor in 100% DMSO (as 10 point duplicate dose response titrations) and allowed to equilibrate at room temperature for 4-5 hours. Reactions were initiated by the addition of 12.5 µL/well of 2 µM biotinylated H3K27me1 substrate peptide (H_2N-RKQLATKAAR(Kme1)SAPATGGVKKP-NTPEGBiot) in the same buffer, and allowed to react at room temperature for 18-22 h. Quenching was accomplished by addition of 20 µL/well of STOP solution (50 mM Tris (pH 8.5), 200 mM EDTA, 2 mM SAH). 35 µl of the quenched solution was transferred to Streptavidin FlashPlates (Perkin Elmer), incubated one hour, washed, and read in a TopCount plate reader (Perkin Elmer). Final DMSO concentration was 0.8% (v/v), and turnover was kept to < 5%. IC_{50} values were calculated using non-linear least squares four parameter fits (Genedata Screener). Due to the high potency, assays were set up under very dilute conditions (pM enzyme/inhibitor) and, even with extended pre-incubation, full equilibration was likely not achieved.

SAM K_m determination

K_m for SAM was determined through incorporation of 3H-SAM into a biotinylated H3 peptide. Specifically, a mixture of 6 nM PRC2 and 3 µM H3K27me3 activating peptide, in a buffer consisting of 50 mM Tris (pH 8.5), 1 mM DTT, 0.07 mM Brij-35, and 0.1 mg/mL BSA, was added at 8.3 µL/well to 384 well plates (Greiner) containing a mixture of 3H-SAM and unlabeled SAM at a ratio of 1:3 in the same buffer, with 2-fold dilutions from 3.8 µM. Reactions were initiated by the addition of 8.3 µL/well of 3 µM H3K27me1 substrate peptide in the same buffer, and allowed to react at room temperature for 1.9 h. Quenching and subsequent product detection was as described in the enzymatic assay above. As the reactions were quenched while still under steady state conditions, final well readings were used as a proxy for initial velocity and fit to the Michaelis-Menten model in Prism 7 (GraphPad).

Enzymatic jump dilution assay

For the 100X jump dilution reaction, PRC2 at 20 nM was pre-incubated with inhibitor at a concentration 100X its apparent K_d for at least 2 hours at room temperature in buffer (50 mM Tris(pH 8.5), 1 mM $MgCl_2$, 4 mM DTT, 0.07 mM Brij-35, 0.1 mg/mL BSA, 1 µM H3K27me3 activating peptide). For the 1X control reaction, PRC2 at 0.2 nM was pre-incubated with inhibitor at a concentration equal to its apparent K_d for at least 2 hours at room temperature in buffer containing 1 µM 3H-SAM and 1 µM unlabeled SAM. To initiate the reactions, the 100X mixture was diluted 100-fold into buffer containing 5 µM biotinylated H3K27me0 substrate peptide, and buffer containing 500 µM biotinylated H3K27me0 was diluted 100-fold into the 1X mixture, both to a final volume of 140 µL in a 384 well polypropylene plate (Greiner). The reactions proceeded for 10 hours at room temperature. At defined time points, an 8 µL aliquot of each

reaction mixture was transferred to an equal volume of STOP solution (50 mM Tris-HCl, 200 mM EDTA, 2 mM SAH, pH 8.5) in a 384 well polystyrene plate (Greiner). After the final time point, 12 µL of the quenched solutions were transferred to a streptavidin coated FlashPlate (PerkinElmer) containing 38 µL STOP solution and allowed to incubate overnight at room temperature. The FlashPlate was then washed and read on a TopCount (PerkinElmer) plate reader. To estimate k_{off}, the 100X jump dilution data were fit to:

$$[\boldsymbol{P}] = \boldsymbol{v_s t} + \frac{\boldsymbol{v_i - v_s}}{\boldsymbol{k_{obs}}}[\mathbf{1} - \boldsymbol{e}^{-\boldsymbol{k_{obs}t}}]$$

V_s was constrained to the slope defined by a linear fit of the 1X control data and k_{obs} was corrected for rebinding using the equation in Supplementary Note I.

SPR characterization

SPR method development and experiments were performed by Beactica Therapeutics (Uppsala, Sweden) on trimeric PRC2 containing EZH2, EED and SUZ12 (BPS Biosciences). Briefly, trimeric PRC2 immobilized by amine coupling to CM7 chips (Cytiva). All experiments were performed using a BiacoreT200 instrument (Cytiva) thermostated at 25°C. The characterization of compound interactions were conducted in a 10 mM Hepes buffer at pH 7.4, with 150 mM NaCl, 2 mM DTT, 0.1 % Pluronic127, 1 % DMSO. For multi-cycle experiments the ligands were injected in increasing concentration series for 15 s at a flow rate of 30 µl/min.

Sensorgrams were double-referenced (reference surface, blanks) prior to global analysis using a simple 1:1 binding model including a term for mass transport limitation. The dissociation constants for slow dissociating compounds were determined using the ExtRA™ method. The determined value for k_{off} was then locked in the global analysis of multi-cycle experiments. In addition, the Rmax value was fitted locally in order to compensate for a progressively blocked surface during the experiment.

TR-FRET k_{off} determination

For non-dialysis k_{off} determinations, PRC2 and Eu(W1024)-α-His antibody (hereafter Eu-α-His, PerkinElmer) were combined in 70 µL assay buffer ((50 mM Hepes (pH 7.4), 100 mM NaCl, 1 mM TCEP, 0.01% Tween-20, 0.1 mg/mL BSA; f.c 120 nM PRC2 and 120 nM Eu-α-His). The resulting 2X mixture was placed in an incubator for ~15 minutes at 25°C. Five microliters of the PRC2:Eu-α-His mixture was transferred to a Greiner 384-well plate. Five microliters of buffer (±) 2x compound and (±) activator peptide was added to respective wells containing PRC2:Eu-α-His mixture (f.c. 70 nM compound, 60 nM PRC2:Eu-α-His mixture, (±) 10 µM activator peptide). Mixtures were incubated for 30 min at 25°C. Five microliters of mixtures were transferred to wells containing 45 µL of 1.1x Biotin-EZH2i (±) activator and mixed thoroughly by pipetting up and down 5-10 times. Ten microliters of diluted mixtures was diluted a second time into 90 µL of 1.1x Biotin-EZH2i (±) activator (f.c. 700 pM EZH2i, 600 pM PRC2:Eu-α-His, 760 nM Biotin EZH2i (±) 10 µM activator peptide). At respective time points, 18 µL of jump dilution mixtures were transferred to black ProxiPlates (PerkinElmer) pre-stamped with 1 µL of 19x SA-APC (PerkinElmer), f.c. 630 pM EZH2i, 540 pM PRC2:Eu-α-His, 684 nM Biotin EZH2i (±) 9 µM activator peptide, 1500 nM SA-APC). Samples were thoroughly mixed by pipetting up and down 5-10 times and then read on an Envision 2104 reader (PerkinElmer) using the manufacturer's recommended filters and settings. The fractional occupancy was determined by comparison to a DMSO only (no inhibitor) and background (no PRC2) controls. Data were fit to an exponential dissociation of the form below. For experiments involving MAK-683, 10 µM (f.c) of MAK-683 was included in compound mixture as well as biotin-EZH2i mixture.

For measurements utilizing dialysis set up: PRC2 inhibitors, activator peptide, and Eu-α-His antibody were combined (V_t 117 µL) and equilibrated overnight (full complex PRC2 [f.c PRC2] 7.5 nM, activator peptide 10 µM, inhibitors 21 nM, Eu-α-His 7.5 nM). Subsequently, the mixture was combined with bio-EZH2i (total volume 175 µL; f.c. PRC2 5 nM, activator peptide 10 µM, inhibitors 14 nM, Eu-α-His 5 nM, bio-

EZH2i 1 µM), transferred to a mini-dialysis chamber (Pierce) and serially dialyzed against several 1.8 mL volumes of buffer (50 mM Hepes (pH 7.4), 100 mM NaCl, 1 mM TCEP, 0.01% Tween-20, 0.1 mg/mL BSA, 0.01% sodium azide) containing 1 µM bio-EZH2i and 10 µM activator peptide. At defined points 4.8 µL aliquots were withdrawn from the dialysis chamber and combined with SA-APC (total volume 40 µL, f.c. PRC2 0.60 nM, activator peptide 10 µM, Eu-α-His 0.60 nM, bio-EZH2i 0.12 µM, SA-APC 1.1 µM) to create the final TR-FRET complex. Plates were incubated for 3-6 min at rt and read. The fractional occupancy was determined by comparison to a DMSO only (no inhibitor) and background (no PRC2) controls, which were subject to the same dialysis conditions. Data were fit to an exponential dissociation of the form:

$$B(t) = \left(B_0 - B_f\right)\left(e^{-k_{off}*t}\right) + B_f$$

where B(t) is the fraction of enzyme bound at time (t), B_0 is the fraction of enzyme bound at t=0, B_f is the fraction of enzyme bound at t= ∞ (constrained to 0), and k_{off} is the dissociation rate constant for inhibitor with PRC2 (in units of t^{-1}).

TR-FRET k_{on} determination

The association rate constants for compounds with EZH2 was determined in an analogous fashion as the dissociation rate constant. In contrast to the dissociation rate constant determinations in which PRC2 and compound were pre-equilibrated, PRC2 and compound were combined and the fraction of bound PRC2 was sampled at different time points using bio-EZH2i to measure the final TR-FRET complex. Specifically, PRC2 (which had been preequilibrated with Eu-α-His) and compound were combined in 50 mM Hepes (pH 7.4), 100 mM NaCl, 1 mM TCEP, 0.01% Tween-20, 0.1 mg/mL BSA, 0.01% sodium azide, and 10 µM H3K27me3 activator peptide in a total volume of 400 µL (f.c. PRC2 1.0 nM, 7.0 nM compound, Eu-α-His 1.0 nM). At defined time points, aliquots (36 µL) were withdrawn and mixed with bio-EZH2i in the same buffer to a final volume of 40 µL (f.c. PRC2 0.90 nM, compound 6.3 nM, Eu-α-His 0.90 nM, bio-EZH2i 1.2 µM). Aliquots of this mixture (36 µL) were then immediately withdrawn and mixed with SA-APC in the same buffer to a final volume of 38 µL (f.c. PRC2 0.85 nM, compound 6.0 nM, Eu-α-His 0.85 nM, bio-EZH2i 1.1 µM, SA-APC 1.5 µM). Plates were incubated for 3-6 minutes at RT and then read (Envision 2104), and the fractional occupancy determined by comparison to a DMSO only (no inhibitor) and background (no bio-EZH2i) controls.

Differential scanning fluorimetry binding assays

Compound potency was assessed through differential scanning fluorimetry (DSF) in a modified TR-FRET assay buffer (50 mM Hepes (pH 7.4), 100 mM NaCl, 1 mM TCEP and 0.2% DMSO). PRC2 was combined with compounds (compounds initially in 100% DMSO) and H3K27me3 activator peptide to final concentrations of 750 nM PRC2, 20 µM compound, 200 µM activating peptide, and 4X PTS Dye (ThermoFisher) in a total volume of 20 µL in a MicroAmp™ EnduraPlate™ Optical 384-Well Clear Reaction Plates with Barcode (Applied Biosystems). The plate was immediately spun at 1000 RPM for ~30 seconds and sealed with a LightCycler® 480 sealing foil (both Roche Diagnostics). After incubation at RT for 90 minutes (to allow full equilibration/binding), plates were analyzed in a Viia7 Real-Time PCR system (ThermoFisher) in a melt curve assay where the temperature was increased from 25°C to 95°C at a rate of 0.05°C/s. Unliganded PRC2 complexes exhibit multiphasic melting transitions as determined by their first derivative melting curves. Melting temperatures (T_mD) were determined using the first derivative melting algorithm in the Protein Thermal Shift™ Analysis software (Applied Biosystems) and ΔT_mD was obtained from $T_mD^{Cmpd} - T_mD^{DMSO\ ctrl}$. Melting temperatures were also determined using the Boltzmann method in the Protein Thermal Shift™ Analysis software (Applied Biosystems, (T_mB)).

Compound mass spectral analysis following incubation with PRC2

PRC2 was buffer exchanged into 50 mM Hepes, pH 7.4, 100 mM NaCl by dialysis (D-Tube™ Dialyzers, MWCO 6-8 kD, Millipore-Sigma) and concentrated to ~6 mg/mL (Amicon Ultra 30k, Millipore-Sigma). Titration of a potent inhibitor in the enzymatic assay showed the concentration of

active enzyme to be 19 μM. Protein/Ligand incubation for MS analyses: final [conc] are PRC2 18.4 μM, 13 10 μM and ± 30 μM H3K27me3 activator peptide with incubation for ~44h at 25°C. Protein samples were denatured with an equal volume of 2% formic acid (FA) for 5min at rt. C18 spin columns (Pierce) were used to desalt protein and compound samples with resin activation with 50% acetonitrile (ACN); equilibration with 5% ACN / 1% FA; wash following sample loading with 5% ACN / 1% FA; elution with 70% ACN / 0.1% FA. Mass spectral analysis was performed on a Synapt G2si HDMS (Waters) equipped with a nano-ESI source. The following instrument setting were used to analyze the samples: Capillary voltage was set to 1kV, source temperature was at 30°C, sampling cone voltage was set to 20V, no nano gas flow was applied. MassLynx v4.2 (Waters) was used for data analysis.

H3K27me3 assessment in HeLa cells

Ten different doses of each test compound (in a series of 3-fold dilutions) were plated in duplicate 384-well tissue culture treated plates (Greiner). HeLa cells grown in culture were trypsinized and counted using a Countess® cell counter (Thermo Fisher). Cells were diluted to 67,000 cells per mL in 10% DMEM (Thermo Fisher) and 15 μL (1,000 cells) were plated into each well using the Biotek MicroFloTM Select Dispenser (BioTek Instruments, Inc.) of the 384-well plate. Plates were incubated at 37 °C /5% CO2 for 72 hrs. One of the duplicate plates was processed for AlphaLISA® and the other for viability. (For AlphaLISA® assays all reagents were PerkinElmer and were used as provided by the manufacturer.) 5 μL per well Cell-Histone Lysis buffer (1X) was added to the plate processed for AlphaLISA® and incubated at RT for 30 min on a plate shaker at low speed. 10 μL per well Histone Extraction buffer was added and the plate further incubated at RT for 20 min on plate shaker with low speed. 10 μL per well of a 5X mix of anti-K27me3 acceptor beads and biotinylated anti-Histone H3 (C-ter) antibody (diluted to 3nM final concentration) was added. The acceptor beads and anti-Histone H3 were diluted in 1X Histone Detection buffer. The plate was sealed and incubated at rt for 1 h. Finally, 10 μL per well of 5X solution of Streptavidin donor beads (20 μg/mL final in 1X Histone Detection Buffer) was added, the plate sealed and incubated at rt for 30 min. The plates were read on an Envision 2104 reader (PerkinElmer) using the manufacturer's recommended filters and settings.

Cell viability was assayed by adding 15 μL of Cell Titer Glo (Promega) to each well with cells with media. The plates were incubated at RT for 15 – 20 minutes on a plate shaker at low speed. Luminescence was read on an Envision 2104 reader (PerkinElmer) using the manufacturer's recommended filters and settings.

Data from both assays was analyzed using Genedata Screener. Readout of DMSO wells were used to normalize the data. Dose–response curves were fit using a four-parameter Hill fit with automated outlier detection and all parameters floating with a constraint on maximal effect ≥−100% activity.

KARPAS-422 GI_{50} assay

Ten different doses of each test compound (in a series of 2-fold dilutions) in triplicate were plated in 96-well Corning™ Costar™ Flat Bottom Cell Culture Plates (Thermo Fisher). Cells were plated at a density of 30,000 cells/well in a total volume of 100 μL/well. Plates were incubated at 37 °C /5% CO_2 for 96 hrs. Sixty microliters of fresh media was added to wells and cells were mixed by pipetting up and down ~15 times. Forty microliters of cell suspension were transferred to a new compound-containing 96-well plate and brought up to a final volume of 100 μL. After 96 hours (day 8), Sixty microliters of fresh media were added to wells and cells were mixed by pipetting up and down ~15 times. Forty microliters of cell suspension were transferred into a 96-well white plate (Corning™ 96-Well White Polystyrene Microplates, ThermoFisher). Equal volume of CellTitre-Glo (Promega) was added to each well. Plates were incubated at RT for 30 min with mild shaking and read as for the HeLa mark assay. Readout of DMSO wells were used to normalize the data. Dose-response data was analyzed using GraphPad Prism and a four-parameter Hill fit.

Animal use care statement

All the procedures were performed according to the guidelines approved by the Institutional Animal Care and Use Committee (IACUC) of WuXi AppTec, Shanghai, China, following the guidance of the Association for Assessment and Accreditation of Laboratory Animal Care (AAALAC).

Efficacy in KARPAS-422 xenograft model

Female CB-17 SCID mice (age 6-8 weeks) were inoculated subcutaneously (SC) at the right flank with the exponentially growing KARPAS-422 tumor cells (5 x 10^6) in 0.2 mL of PBS with Matrigel (1:1) at WuXi AppTech(Shanghai). The treatment was started on day 24 after tumor inoculation. Vehicle-treated mice (20% Propylene Glycol (PG) +10% Solutol HS15+70% 50 mM phthalate buffer (pH = 3.5), 29 days) consisted of 7 randomly assigned tumor-bearing mice. Seven mice were treated with CPI-1328 25 mg/kg PO QD (27 days) while six mice respectively were treated with CPI-1328 10 mg/kg PO QD (27 days), 25 mg/kg PO QD Tazemetostat (29 days) and 160 mg/kg PO BID Tazemetostat (29 days). Mice were dosed until the tumor volume reached 2000 mm^3 as per IACUC guidelines. Each group consisted of randomly assigned tumor-bearing mice. Three mice from each sample group were taken down at day 12 for PK/PD analysis. Tumor size was measured three times a week using a caliper, and the tumor volume (V) was expressed in mm3 using the formula: V = 0.5a × b2 where “a” and “b” are the long and short diameters of the tumor, respectively. The mice were weighed every day. TGI % was calculated according to the following equation: TGI (%) = [1-(T1-T0) / (C1-C0)] × 100, where C1- mean tumor volume of control mice at time t; T1 -mean tumor volume of treated mice at time t; C0-mean tumor volume of control mice at time 0; T0-means tumor volume of treated mice at time 0.

Tumor pharmacodynamic assay

H3K27me3 and total H3 expression levels in tumors was analyzed by Meso Scale Discovery (MSD) ELISA. Briefly, each tumor was collected after animal euthanization, snap-frozen in liquid nitrogen and then transferred to -80°C before analysis. Approximately 20-30 mg of tissue was transferred in 2 mL Eppendorf tubes. Four hundred microliters of 1X RIPA buffer supplemented with 1X complete protease inhibitor cocktail, 1 mM PMSF and 1:5000 Benzonase® was added. Tumors were ground with a Tissuelyser LT at full speed for 5 min. Samples were incubated on ice for 30 min. to each sample, one hundred microliters of 5M NaCl was added (1 M f.c.). Samples were mixed 3-5 times with a pipet and briefly vortexed. Samples were sonicated 2x for 30s at max output power with biorupt UCD-200 (Diagenode). Samples were incubated on ice for 30 min followed by centrifugation for 10 min at 12000 x g. Supernatants were transferred to a new vial and protein concentration was determined via the BCA method. Lysates were diluted to a final concentration of 0.25 µg/µL using 1X RIPA buffer containing 1M NaCl. Lysates can be stored frozen at -80°C. MSD standard bind 96-well plates were coated with 30 µL total histone H3 capture antibody at 1 µg/mL in PBS (EMD-MAB3422). Plates were sealed and left overnight at 4°C. Coating buffer was removed and plates were washed 3X with 150 µL of TBST. Plates were blocked with 150 µL of 5% BSA in 1X TBST at RT with shaking for 1h. Blocking buffer was removed and plates were washed 3X with 150 µL of TBST. Lysates were diluted to a final concentration of 0.025 µg/µL per well using buffer lacking salt or detergent (sodium concentration reduced to ~100 mM). Twenty-five microliters of each sample was loaded into an individual well. Plates were incubated with lysates for 2h at RT with shaking. Lysates were removed and plates were washed 3X with 150 µL of TBST. Twenty-five microliters of αH3K27me3 (0.25 µg/mL, Cell Signaling 9733) which had previously been validated in-house (49) or anti-Histone H3 (0.125 µg/mL, Cell Signaling 4499) in 1% BSA in TBST were added for 30 min at RT with shaking. Twenty-five microliters per well of sulfo-tag rabbit antibody (MSD Catalog# R32AB-1) in 1% BSA in TBST (0.5 µg/mL) were added followed by incubation for 1h at RT with shaking. Antibody mixtures were removed from wells and samples were washed 3X with 150 µL of TBST. Reading buffer (1X) was added to wells (150 µL) and plates were read on an MSD instrument.

Data Availability: All data are contained within the article. For compounds that are not commercially available detailed syntheses and characterization are found in the Supporting Information. Additionally, a comprehensive summary of biochemical data collected for each compound and presented here can be found in Supplemental Tables I-III.

Acknowledgements

Surface plasmon resonance studies were carried out under the direction of Per Källblad and Matthis Geitmann at Beactica AB (Uppsala, Sweden). Mass spectrometric analyses were performed on instrumentation at the UMass Amherst Mass Spectrometry Center which is under the direction of Dr. Stephen Eyles who also provided helpful technical advice. We would also like to acknowledge our collaborators at WuXi AppTec for compound syntheses and animal studies. Lastly, we would like to thank our colleague Leslie Dakin for the synthesis of the biotinylated probe compound.

Conflict of Interest: The authors declare no conflicts of interest in regard to this manuscript.

References

1. Strahl, B. D., and Allis, C. D. (2000) The language of covalent histone modifications. *Nature* **403**, 41-45

2. Jenuwein, T., and Allis, C. D. (2001) Translating the histone code. *Science* **293**, 1074-1080

3. Bannister, A. J., and Kouzarides, T. (2011) Regulation of chromatin by histone modifications. *Cell Res* **21**, 381-395

4. Chi, P., Allis, C. D., and Wang, G. G. (2010) Covalent histone modifications--miswritten, misinterpreted and mis-erased in human cancers. *Nat Rev Cancer* **10**, 457-469

5. Koschmann, C., Nunez, F. J., Mendez, F., Brosnan-Cashman, J. A., Meeker, A. K., Lowenstein, P. R., and Castro, M. G. (2017) Mutated Chromatin Regulatory Factors as Tumor Drivers in Cancer. *Cancer Res* **77**, 227-233

6. Zhao, L., Duan, Y. T., Lu, P., Zhang, Z. J., Zheng, X. K., Wang, J. L., and Feng, W. S. (2018) Epigenetic Targets and their Inhibitors in Cancer Therapy. *Curr Top Med Chem* **18**, 2395-2419

7. Tanaka, M., Roberts, J. M., Qi, J., and Bradner, J. E. (2015) Inhibitors of emerging epigenetic targets for cancer therapy: a patent review (2010-2014). *Pharm Pat Anal* **4**, 261-284

8. Kim, K. H., and Roberts, C. W. (2016) Targeting EZH2 in cancer. *Nat Med* **22**, 128-134

9. Yap, D. B., Chu, J., Berg, T., Schapira, M., Cheng, S. W., Moradian, A., Morin, R. D., Mungall, A. J., Meissner, B., Boyle, M., Marquez, V. E., Marra, M. A., Gascoyne, R. D., Humphries, R. K., Arrowsmith, C. H., Morin, G. B., and Aparicio, S. A. (2011) Somatic mutations at EZH2

Y641 act dominantly through a mechanism of selectively altered PRC2 catalytic activity, to increase H3K27 trimethylation. *Blood* **117**, 2451-2459

10. Majer, C. R., Jin, L., Scott, M. P., Knutson, S. K., Kuntz, K. W., Keilhack, H., Smith, J. J., Moyer, M. P., Richon, V. M., Copeland, R. A., and Wigle, T. J. (2012) A687V EZH2 is a gain-of-function mutation found in lymphoma patients. *FEBS Lett* **586**, 3448-3451

11. McCabe, M. T., Graves, A. P., Ganji, G., Diaz, E., Halsey, W. S., Jiang, Y., Smitheman, K. N., Ott, H. M., Pappalardi, M. B., Allen, K. E., Chen, S. B., Della Pietra, A., 3rd, Dul, E., Hughes, A. M., Gilbert, S. A., Thrall, S. H., Tummino, P. J., Kruger, R. G., Brandt, M., Schwartz, B., and Creasy, C. L. (2012) Mutation of A677 in histone methyltransferase EZH2 in human B-cell lymphoma promotes hypertrimethylation of histone H3 on lysine 27 (H3K27). *Proc Natl Acad Sci U S A* **109**, 2989-2994

12. Gan, L., Yang, Y., Li, Q., Feng, Y., Liu, T., and Guo, W. (2018) Epigenetic regulation of cancer progression by EZH2: from biological insights to therapeutic potential. *Biomark Res* **6**, 10

13. Gulati, N., Beguelin, W., and Giulino-Roth, L. (2018) Enhancer of zeste homolog 2 (EZH2) inhibitors. *Leuk Lymphoma* **59**, 1574-1585

14. Stazi, G., Zwergel, C., Mai, A., and Valente, S. (2017) EZH2 inhibitors: a patent review (2014-2016). *Expert Opin Ther Pat* **27**, 797-813

15. Danishuddin, Subbarao, N., Faheem, M., and Khan, S. N. (2019) Polycomb repressive complex 2 inhibitors: emerging epigenetic modulators. *Drug Discov Today* **24**, 179-188

16. Bratkowski, M., Yang, X., and Liu, X. (2018) An Evolutionarily Conserved Structural Platform for PRC2 Inhibition by a Class of Ezh2 Inhibitors. *Sci Rep* **8**, 9092

17. Brooun, A., Gajiwala, K. S., Deng, Y. L., Liu, W., Bolanos, B., Bingham, P., He, Y. A., Diehl, W., Grable, N., Kung, P. P., Sutton, S., Maegley, K. A., Yu, X., and Stewart, A. E. (2016) Polycomb repressive complex 2 structure with inhibitor reveals a mechanism of activation and drug resistance. *Nat Commun* **7**, 11384

18. Vaswani, R. G., Gehling, V. S., Dakin, L. A., Cook, A. S., Nasveschuk, C. G., Duplessis, M., Iyer, P., Balasubramanian, S., Zhao, F., Good, A. C., Campbell, R., Lee, C., Cantone, N., Cummings, R. T., Normant, E., Bellon, S. F., Albrecht, B. K., Harmange, J. C., Trojer, P., Audia, J. E., Zhang, Y., Justin, N., Chen, S., Wilson, J. R., and Gamblin, S. J. (2016) Identification of (R)-N-((4-Methoxy-6-methyl-2-oxo-1,2-dihydropyridin-3-yl)methyl)-2-methyl-1-(1-(1 -(2,2,2-trifluoroethyl)piperidin-4-yl)ethyl)-1H-indole-3-carboxamide (CPI-1205), a Potent and Selective Inhibitor of Histone Methyltransferase EZH2, Suitable for Phase I Clinical Trials for B-Cell Lymphomas. *J Med Chem* **59**, 9928-9941

19. Xu, C., Bian, C., Yang, W., Galka, M., Ouyang, H., Chen, C., Qiu, W., Liu, H., Jones, A. E., MacKenzie, F., Pan, P., Li, S. S., Wang, H., and Min, J. (2010) Binding of different histone marks differentially regulates the activity and specificity of polycomb repressive complex 2 (PRC2). *Proc Natl Acad Sci U S A* **107**, 19266-19271

20. Hansen, K. H., Bracken, A. P., Pasini, D., Dietrich, N., Gehani, S. S., Monrad, A., Rappsilber, J., Lerdrup, M., and Helin, K. (2008) A model for transmission of the H3K27me3 epigenetic mark. *Nat Cell Biol* **10**, 1291-1300

21. Qi, W., Zhao, K., Gu, J., Huang, Y., Wang, Y., Zhang, H., Zhang, M., Zhang, J., Yu, Z., Li, L., Teng, L., Chuai, S., Zhang, C., Zhao, M., Chan, H., Chen, Z., Fang, D., Fei, Q., Feng, L., Feng, L., Gao, Y., Ge, H., Ge, X., Li, G., Lingel, A., Lin, Y., Liu, Y., Luo, F., Shi, M., Wang, L., Wang, Z., Yu, Y., Zeng, J., Zeng, C., Zhang, L., Zhang, Q., Zhou, S., Oyang, C., Atadja, P., and Li, E. (2017) An allosteric PRC2 inhibitor targeting the H3K27me3 binding pocket of EED. *Nat Chem Biol* **13**, 381-388

22. He, Y., Selvaraju, S., Curtin, M. L., Jakob, C. G., Zhu, H., Comess, K. M., Shaw, B., The, J., Lima-Fernandes, E., Szewczyk, M. M., Cheng, D., Klinge, K. L., Li, H. Q., Pliushchev, M., Algire, M. A., Maag, D., Guo, J., Dietrich, J., Panchal, S. C., Petros, A. M., Sweis, R. F., Torrent, M., Bigelow, L. J., Senisterra, G., Li, F., Kennedy, S., Wu, Q., Osterling, D. J., Lindley, D. J., Gao, W., Galasinski, S., Barsyte-Lovejoy, D., Vedadi, M., Buchanan, F. G., Arrowsmith, C. H., Chiang, G. G., Sun, C., and Pappano, W. N. (2017) The EED protein-protein interaction inhibitor A-395 inactivates the PRC2 complex. *Nat Chem Biol* **13**, 389-395

23. Van Aller, G. S., Pappalardi, M. B., Ott, H. M., Diaz, E., Brandt, M., Schwartz, B. J., Miller, W. H., Dhanak, D., McCabe, M. T., Verma, S. K., Creasy, C. L., Tummino, P. J., and Kruger, R. G. (2014) Long residence time inhibition of EZH2 in activated polycomb repressive complex 2. *ACS Chem Biol* **9**, 622-629

24. Motulsky, H. J., and Mahan, L. C. (1984) The kinetics of competitive radioligand binding predicted by the law of mass action. *Mol Pharmacol* **25**, 1-9

25. Copeland, R. A. (2016) The drug-target residence time model: a 10-year retrospective. *Nat Rev Drug Discov* **15**, 87-95

26. Copeland, R. A., Pompliano, D. L., and Meek, T. D. (2006) Drug-target residence time and its implications for lead optimization. *Nat Rev Drug Discov* **5**, 730-739

27. Tummino, P. J., and Copeland, R. A. (2008) Residence time of receptor-ligand complexes and its effect on biological function. *Biochemistry* **47**, 5481-5492

28. Quinn, J. G., Pitts, K. E., Steffek, M., and Mulvihill, M. M. (2018) Determination of Affinity and Residence Time of Potent Drug-Target Complexes by Label-free Biosensing. *J Med Chem* **61**, 5154-5161

29. Khanna, A., Cote, A., Arora, S., Moine, L., Gehling, V. S., Brenneman, J., Cantone, N., Stuckey, J. I., Apte, S., Ramakrishnan, A., Bruderek, K., Bradley, W. D., Audia, J. E., Cummings, R. T., Sims, R. J., 3rd, Trojer, P., and Levell, J. R. (2020) Design, Synthesis, and Pharmacological Evaluation of Second Generation EZH2 Inhibitors with Long Residence Time. *ACS Med Chem Lett* **11**, 1205-1212

30. Copeland, R. A., Basavapathruni, A., Moyer, M., and Scott, M. P. (2011) Impact of enzyme concentration and residence time on apparent activity recovery in jump dilution analysis. *Anal Biochem* **416**, 206-210

31. Yung-Chi, C., and Prusoff, W. H. (1973) Relationship between the inhibition constant (KI) and the concentration of inhibitor which causes 50 per cent inhibition (I50) of an enzymatic reaction. *Biochemical Pharmacology* **22**, 3099-3108

32. Konze, K. D., Ma, A., Li, F., Barsyte-Lovejoy, D., Parton, T., Macnevin, C. J., Liu, F., Gao, C., Huang, X. P., Kuznetsova, E., Rougie, M., Jiang, A., Pattenden, S. G., Norris, J. L., James, L. I., Roth, B. L., Brown, P. J., Frye, S. V., Arrowsmith, C. H., Hahn, K. M., Wang, G. G., Vedadi, M., and Jin, J. (2013) An orally bioavailable chemical probe of the Lysine Methyltransferases EZH2 and EZH1. *ACS Chem Biol* **8**, 1324-1334

33. McPherson, R. A., and Zettner, A. (1975) A mathematical analysis of the incubation time in competitive binding systems. *Analytical Biochemistry* **64**, 501-508

34. Hlavacek, W. S. Analytical results for a reversible bimolecular association reaction.

35. Benson, S. W. (1960) *The Foundations of Chemical Kinetics*, McGraw-Hill Book Company, New York

36. Boeker, E. A. (1984) Simple integrated rate equations for reversible bimolecular reactions. *Experientia* **40**, 453-456

37. Gonzalez, M., Bagatolli, L. A., Echabe, I., Arrondo, J. L., Argarana, C. E., Cantor, C. R., and Fidelio, G. D. (1997) Interaction of biotin with streptavidin. Thermostability and conformational changes upon binding. *J Biol Chem* **272**, 11288-11294

38. Overington, J. P., Al-Lazikani, B., and Hopkins, A. L. (2006) How many drug targets are there? *Nat Rev Drug Discov* **5**, 993-996

39. Smith, A. J., Zhang, X., Leach, A. G., and Houk, K. N. (2009) Beyond picomolar affinities: quantitative aspects of noncovalent and covalent binding of drugs to proteins. *J Med Chem* **52**, 225-233

40. Kung, P. P., Bingham, P., Brooun, A., Collins, M., Deng, Y. L., Dinh, D., Fan, C., Gajiwala, K. S., Grantner, R., Gukasyan, H. J., Hu, W., Huang, B., Kania, R., Kephart, S. E., Krivacic, C., Kumpf, R. A., Khamphavong, P., Kraus, M., Liu, W., Maegley, K. A., Nguyen, L., Ren, S., Richter, D., Rollins, R. A., Sach, N., Sharma, S., Sherrill, J., Spangler, J., Stewart, A. E., Sutton, S., Uryu, S., Verhelle, D., Wang, H., Wang, S., Wythes, M., Xin, S., Yamazaki, S., Zhu, H., Zhu, J., Zehnder, L., and Edwards, M. (2018) Optimization of Orally Bioavailable Enhancer of Zeste Homolog 2 (EZH2) Inhibitors Using Ligand and Property-Based Design Strategies: Identification of Development Candidate (R)-5,8-Dichloro-7-(methoxy(oxetan-3-yl)methyl)-2-((4-methoxy-6-methyl-2-oxo-1,2- dihydropyridin-3-yl)methyl)-3,4-dihydroisoquinolin-1(2H)-one (PF-06821497). *J Med Chem* **61**, 650-665

41. Honma, D., Kanno, O., Watanabe, J., Kinoshita, J., Hirasawa, M., Nosaka, E., Shiroishi, M., Takizawa, T., Yasumatsu, I., Horiuchi, T., Nakao, A., Suzuki, K., Yamasaki, T., Nakajima, K., Hayakawa, M., Yamazaki, T., Yadav, A. S., and Adachi, N. (2017) Novel orally bioavailable EZH1/2 dual inhibitors with greater antitumor efficacy than an EZH2 selective inhibitor. *Cancer Sci* **108**, 2069-2078

42. Kuntz, I. D., Chen, K., Sharp, K. A., and Kollman, P. A. (1999) The maximal affinity of ligands. *Proc Natl Acad Sci U S A* **96**, 9997-10002

43. Bull, H. G., Garcia-Calvo, M., Andersson, S., Baginsky, W. F., Chan, H. K., Ellsworth, D. E., Miller, R. R., Stearns, R. A., Bakshi, R. K., Rasmusson, G. H., Tolman, R. L., Myers, R. W., Kozarich, J. W., and Harris, G. S. (1996) Mechanism-Based Inhibition of Human Steroid 5α-

Reductase by Finasteride: Enzyme-Catalyzed Formation of NADP−Dihydrofinasteride, a Potent Bisubstrate Analog Inhibitor. *Journal of the American Chemical Society* **118**, 2359-2365

44. Schloss, J. V. (1988) Comparative affinities of the epimeric reaction-intermediate analogs 2- and 4-carboxy-D-arabinitol 1,5-bisphosphate for spinach ribulose 1,5-bisphosphate carboxylase. *J Biol Chem* **263**, 4145-4150

45. Kaplan, A. P., and Bartlett, P. A. (1991) Synthesis and evaluation of an inhibitor of carboxypeptidase A with a Ki value in the femtomolar range. *Biochemistry* **30**, 8165-8170

46. Kim, H., and Lipscomb, W. N. (1991) Comparison of the structures of three carboxypeptidase A-phosphonate complexes determined by X-ray crystallography. *Biochemistry* **30**, 8171-8180

47. Beno, B. R., Yeung, K. S., Bartberger, M. D., Pennington, L. D., and Meanwell, N. A. (2015) A Survey of the Role of Noncovalent Sulfur Interactions in Drug Design. *J Med Chem* **58**, 4383-4438

48. Valley, C. C., Cembran, A., Perlmutter, J. D., Lewis, A. K., Labello, N. P., Gao, J., and Sachs, J. N. (2012) The methionine-aromatic motif plays a unique role in stabilizing protein structure. *J Biol Chem* **287**, 34979-34991

49. Garapaty-Rao, S., Nasveschuk, C., Gagnon, A., Chan, Eric Y., Sandy, P., Busby, J., Balasubramanian, S., Campbell, R., Zhao, F., Bergeron, L., Audia, James E., Albrecht, Brian K., Harmange, J.-C., Cummings, R., and Trojer, P. (2013) Identification of EZH2 and EZH1 Small Molecule Inhibitors with Selective Impact on Diffuse Large B Cell Lymphoma Cell Growth. *Chemistry & Biology* **20**, 1329-1339

Figure Legends

Figure 1. Comparison of SPR-determined residence times and residence times determined using modified jump dilution methodology. Close agreement between the two methodologies was observed for all compounds in this set with GSK126 presenting the most significant divergence as a result of a comparatively short residence time under these conditions. Data are individual replicates with error bars representing the standard deviation of the mean.

Figure 2. Characterization of EZH2i using a TR-FRET binding assay. All data are in the context of basal PRC2. **A.** Biotin-EZH2i used in TR-FRET methodology. **B.** Depiction of final complex observed using TR-FRET readout. **C.** Example PRC2-EZH2i dissociation curve measured using TR-FRET based methodology. Data are plotted as the average of 2 technical replicates with error bars representing the standard deviation of the mean. **D.** Example PRC2-EZH2i association curves measured using TR-FRET based methodology. Data are plotted as the average of 2 technical replicates with error bars representing the standard deviation of the mean. **E.** Comparison of residence time values obtained in SPR and TR-FRET assay formats. Data are individual replicates with error bars representing the standard deviation of the mean. **F.** Comparison of association rate constant values obtained in SPR and TR-FRET assay formats. Data are individual replicates with error bars representing the standard deviation of the mean. **G.** Comparison of calculated inhibitor dissociation constant values obtained from kinetic parameters in either SPR or TR-FRET assay formats from the data displayed in E and F ($K_i = \frac{k_{off}}{k_{on}}$) where error bars represent propagated error.

Figure 3. Exploration of allosteric modulation of EZH2i potencies. **A.** Effect of allosteric modulation on inhibitor residence times for EZH2 inhibitors used to develop kinetic methodologies. Error bars represent propagated error from measured values used in calculation. **B.** Modulation of CPI-1205 residence time by MAK683 (EEDi). Representative data are plotted as the average of 2 technical replicates (±) standard deviation. The residence time of CPI-1205 for basal PRC2 is 1.2 ± 0.3 hours (mean ± SD of 9 biological replicates each in duplicate). For basal PRC2 in the presence of 10 μM MAK683, the residence time of CPI-1205 is 0.97 ± 0.1 hr (average ± SD of 3 biological replicates each in duplicate). **C.** MAK683 (10 μM) inhibition of CPI-1205 residence time enhancement by H3K27me3 activator peptide (10 μM). Representative data are plotted as the average of 2 technical replicates ± standard deviation. The residence time of CPI-1205 PRC2 in the presence of H3K27me3 activator peptide and MAK-683 (10 mM each) is 1.3 ± 0.2 hours (mean ± SD of 4 biological replicates each in duplicate). **D.** Comparison of association rate constant values of EZH2i (±) 10 μM H3K27me3 activator peptide. Data are individual replicates with error bars representing the standard deviation of the mean. **E.** and **F.** Plots of residence time values for basal (E; R^2 0.78) and activated (F; R^2 0.82) PRC2 vs pEC_{50} values for H3K27me3 mark reduction in HeLa cells.

Figure 4. Universal enhancement of EZH2i residence time by 4-thiomethyl pyridone substitution. **A.** and **B.** Residence time comparison of CPI-1205 with its matched pair, 4-thiomethyl analog 2. Data in B are representative data with each point being the average of duplicates and error bars the standard deviation of the mean. **C.** and **D.** Structure of alternative indole scaffold explored during inhibitor development efforts and residence time values for various functional group substitutions at the 4-position of the pyridone moiety, respectively. For D data are individual replicates with error bars representing the standard deviation of the mean.. **E.** 4-thiomethyl pyridone substitution leads to residence time enhancements for clinical stage EZH2i. Error bars represent propagated error from measured values used in calculation.

Figure 5. Characterization of high affinity EZH2i. **A.** and **B.** Contribution of individual kinetic parameters to compound binding affinities. **C.** Structure of sub-pM, S-methyl-containing EZH2i, 13. **D.** Representative dissociation curve for 13. Data are plotted as the average of 2 technical replicates with error bars being the standard deviation of the mean: τ = 2,300 ± 300 hours (mean ± SD, 5 biological replicates each performed in duplicate). **E.** Thermal melt curve plots of selected EZH2 inhibitors (N=3 for each sample). $\Delta T_m D$ (mean ± SEM (°C)): CPI-1205 (11.54 ± 0.05); **2** (13.69 ± 0.00); DS-3201b (14.66 ± 0.00); **13** (15.78 ± 0.00) **F.** Correlation of $\Delta T_m D$ with kinetically determined pK_i for EZH2i.

Figure 6. Residence time enhancement driven through rational design. **A.** Conformational restriction of 13 to produce CPI-1328. K_i values were calculated from kinetic parameters displayed in B. **B.** Comparison of kinetic parameters for 13 and CPI-1328. Error bars represent the standard deviation of the measurements. For 13: k_{on} = 9.1 (± 3) x 10^5 M^{-1} s^{-1}; τ = 2,300 ± 300 hr. For CPI-1328: k_{on} = 1.0 (± 0.2) x 10^6 M^{-1} s^{-1}; τ = 4,400 ± 200.

Figure 7. Biological characterization of 2nd Gen EZH2i. **A.** Plot of inhibitor residence time values vs EC_{50} values for H3K27me3 reduction in HeLa cells. **B.** Plot of inhibitor residence time values vs GI_{50} values for KARPAS-422 cell line. **C.** Plot of inhibitor pK_i values vs GI_{50} values in KARPAS-422 cell line. **D.** Modulation of global H3K27me3 levels (Day 12) in a Karpas-422 xenograft model by CPI-1328 and EPZ-6438. Data are individual replicates with error bars representing the standard deviation of the mean. **E.** and **F.** Efficacy of CPI-1328 and EPZ-6438 in a Karpas-422 xenograft model, respectively. Data are the average of three or more animals with error bars representing the standard error of the mean.

Figure 1

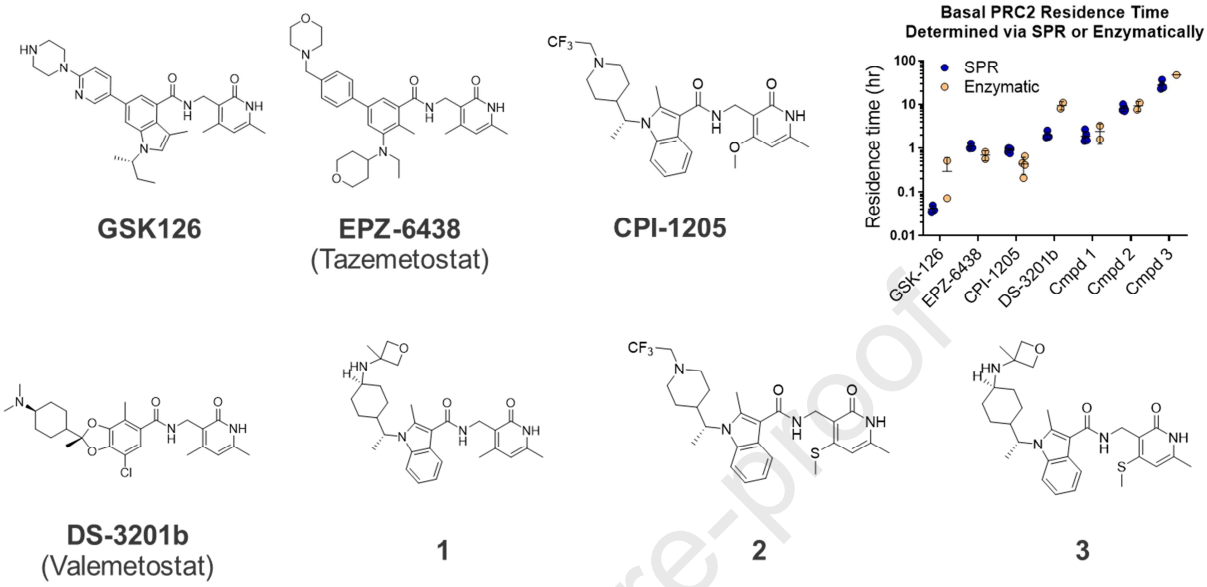

Figure 2

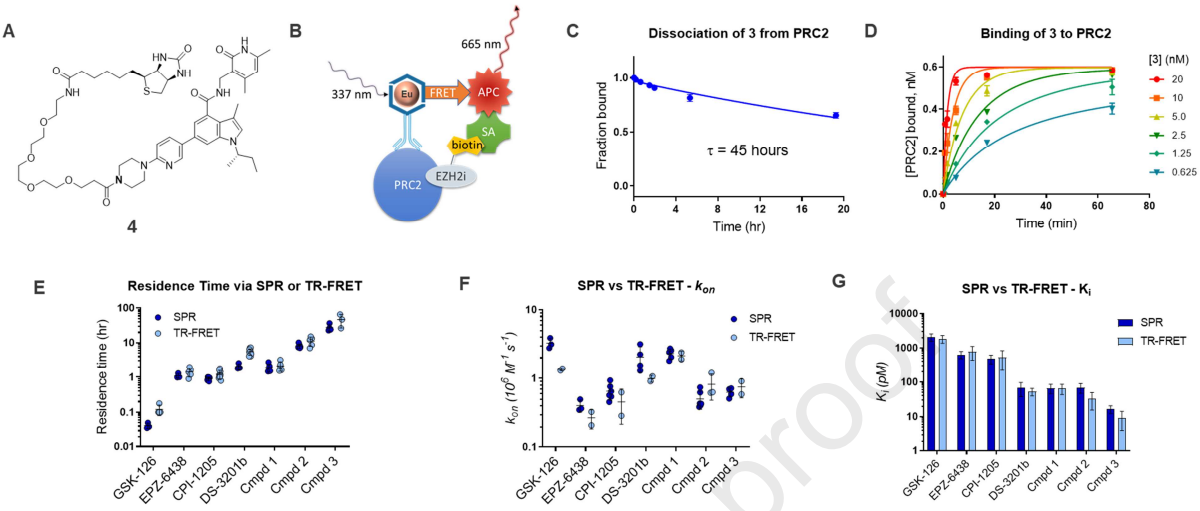

Figure 3

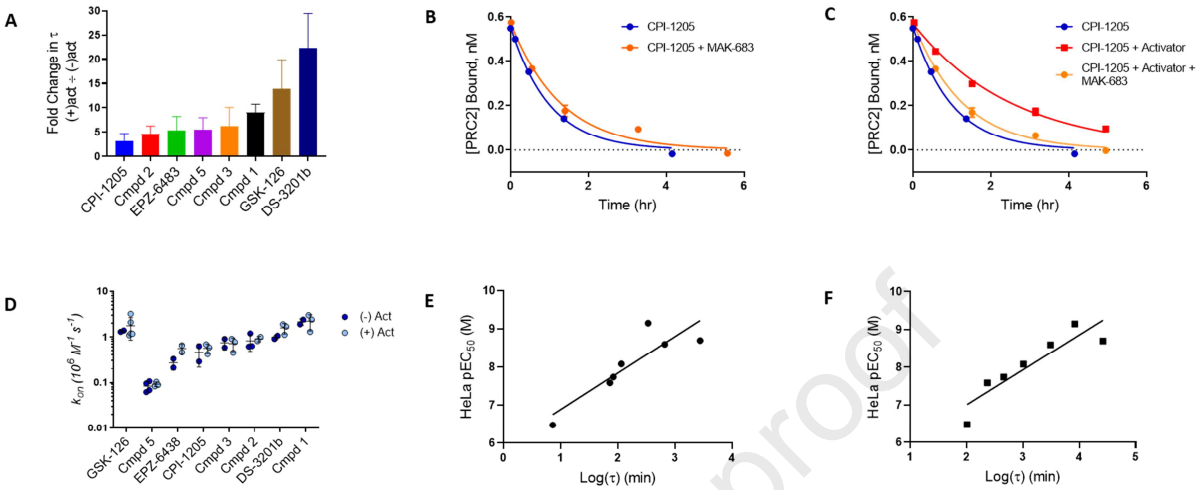

Figure 4

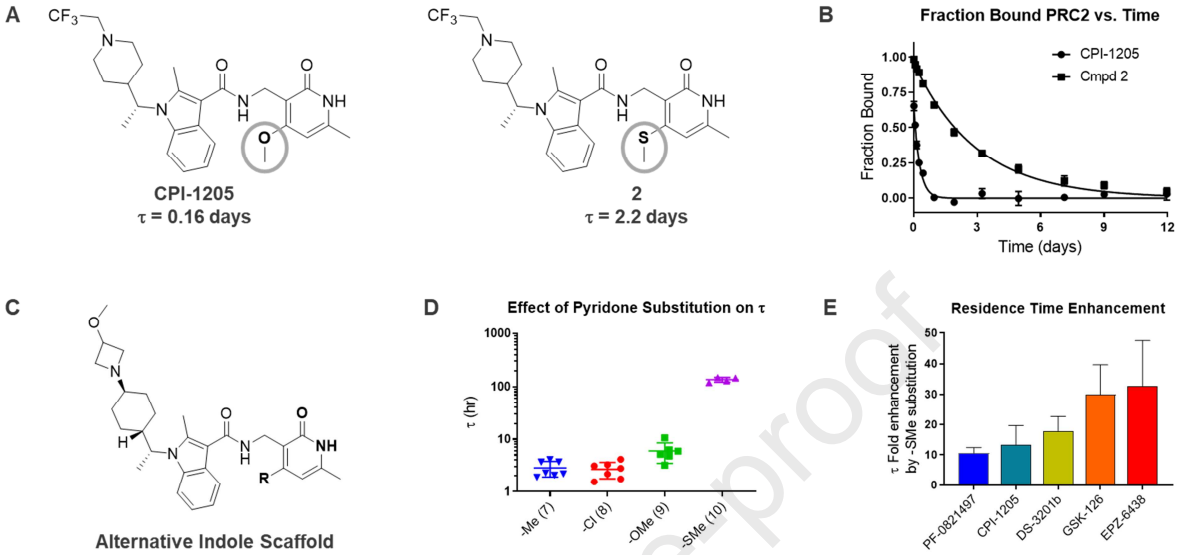

Figure 5

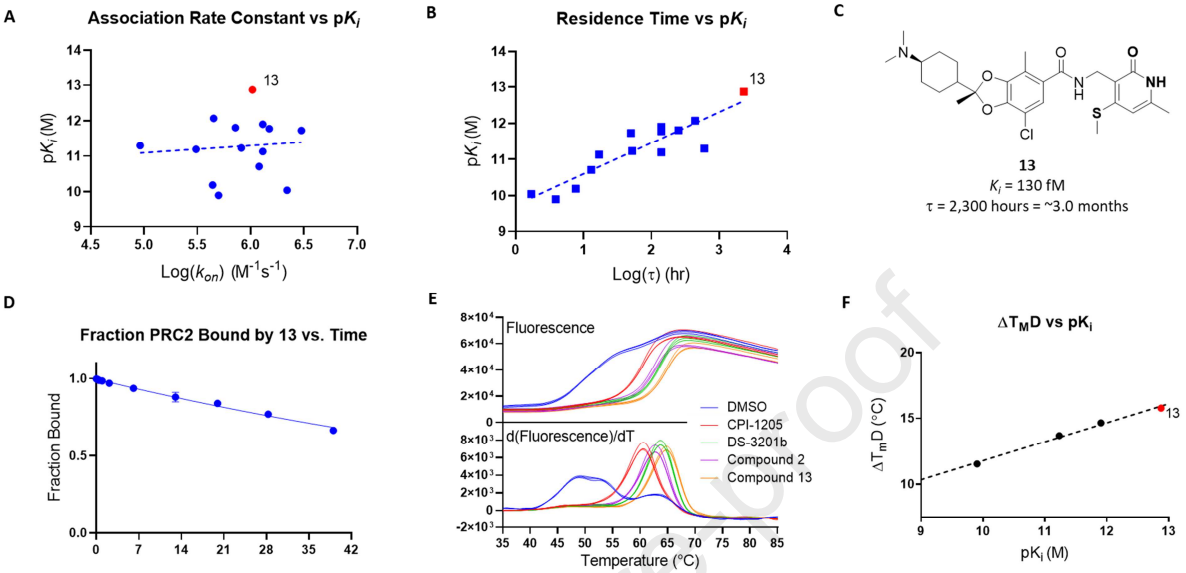

Figure 6

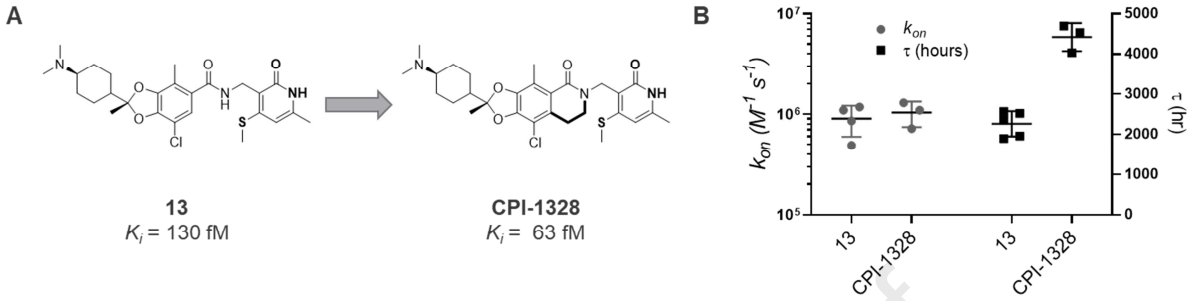

Figure 7

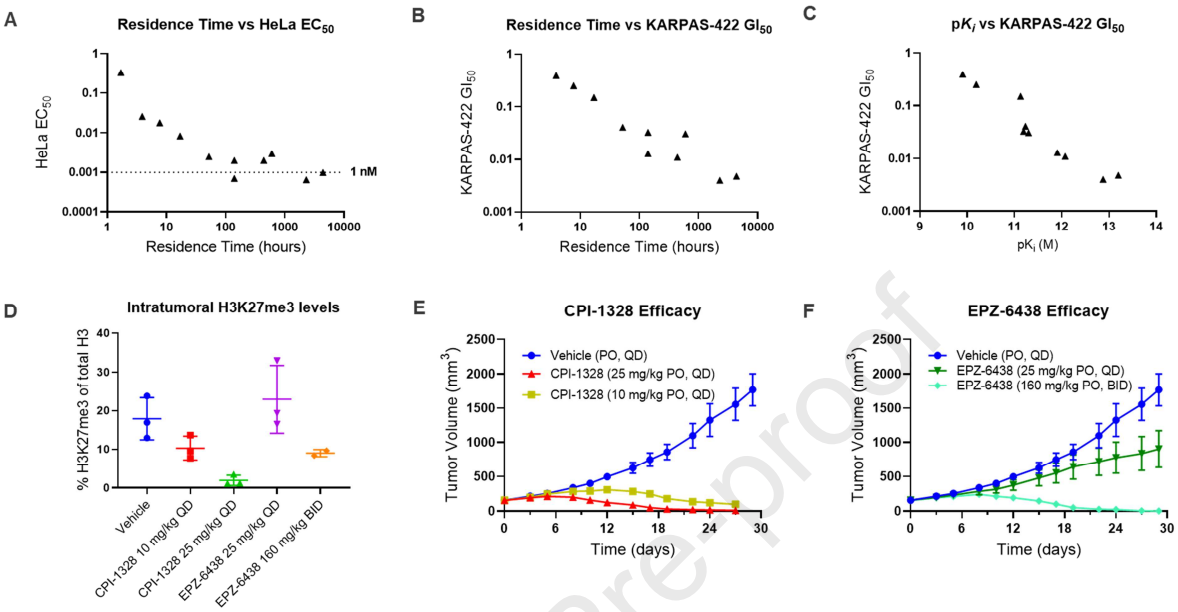

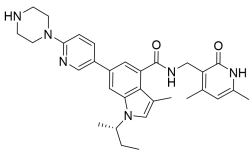

GSK126

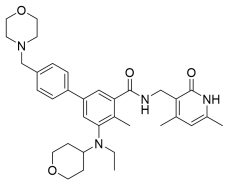

EPZ-6438
(Tazemetostat)

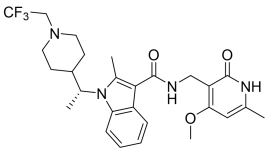

CPI-1205

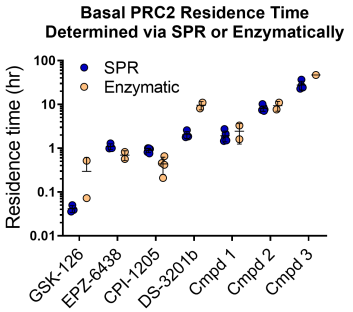

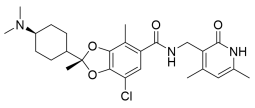

DS-3201b
(Valemetostat)

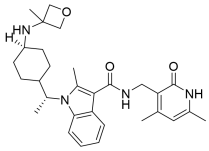

1

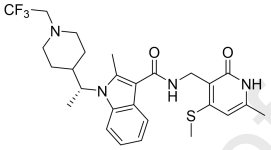

2

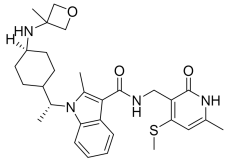

3